2021 60th IEEE Conference on Decision and Control (CDC)
December 13-15, 2021. Austin, Texas

Global trajectory tracking for quadrotors: An MRP-based hybrid backstepping strategy

Luís Martins, Carlos Cardeira, and Paulo Oliveira

Abstract— **In this paper, a novel control strategy is proposed to solve the trajectory tracking problem for quadrotors. The control strategy consists of a hybrid backstepping controller, designed considering the modified Rodrigues parameters attitude description, that comprises a saturated position control law. The hybrid nature of the controller enables overcoming the global stabilizing continuous feedback topological obstruction. Moreover, it provides a suitable framework to capitalize on the unique properties of the referred attitude description. The resulting solution is robust to small measurement noise and, for any given initial state of the vehicle, is able to asymptotically track a position trajectory satisfying some assumptions while minimizing the distance to the desired attitude. The simulation results demonstrate and validate the potential of the strategy.**

I. INTRODUCTION

Over the past decade, unmanned aerial vehicles (UAVs) have been considered for an increasingly broad spectrum of applications. In parallel, the research community has devoted multiple projects to explore and extend the potential and features of these vehicles. Within the UAVs, the quadrotor is one of the most resorted for experimentation of control and navigation strategies due to its maneuverability, hovering capacity, and reduced size.

A vast multitude of control solutions, exploiting different attitude representations, can be found in the literature. The representation in terms of Euler angles is often used to parameterize the attitude. However, it constitutes a hindrance in attaining a global asymptotic stability result in virtue of its singularities and redundancy. Alternatively, state-of-the-art works demonstrate the feasibility of achieving global attitude tracking by resorting to a strategy relying on unit quaternion [1] or rotation matrix representations [2]. In addition to these mainstream representations, the modified Rodrigues parameters (MRP) constitute a more recent attitude description that has been less explored in the context of UAVs. Two numerically different sets characterize the MRP representation. The original and the shadow sets result from the stereographic projection of the unit quaternion and its antipodal onto a three-dimensional hyperplane, respectively. Since these sets are singular for different rotations, a minimal non-singular attitude representation can be obtained by judiciously switching between them [3]. In [4], the authors proposed a global attitude control strategy based on this representation.

L. Martins is with the Institute of Mechanical Engineering, Instituto Superior Técnico, Universidade de Lisboa, Lisboa, Portugal luis.cunha.martins@tecnico.ulisboa.pt

C. Cardeira is with the Institute of Mechanical Engineering, Instituto Superior Técnico, Universidade de Lisboa, Lisboa, Portugal carlos.cardeira@tecnico.ulisboa.pt

P. Oliveira is with the Institute of Mechanical Engineering and the Institute for Systems and Robotics, Instituto Superior Técnico, Universidade de Lisboa, Lisboa, Portugal paulo.j.oliveira@tecnico.ulisboa.pt

Several control solutions relying on continuous feedback laws have been proposed to tackle the quadrotor trajectory tracking problem [5], [6], [7]. However, as demonstrated in [8], it is not possible to attain a global tracking result through continuous feedback. Thus, more recent works report control methodologies developed within the hybrid systems theory framework to overcome this well-known topological obstacle. For attitude tracking, [1], [2], [4] are examples of hybrid solutions. In [9], the authors propose a robust quaternion-based hybrid controller for trajectory tracking that comprises a robust saturated position controller. The strategy extends the attitude controller presented in [1] by applying the backstepping technique and the dynamic path lifting algorithm proposed in [10]. In [11], the authors designed a robust hierarchical control structure for global trajectory tracking. This methodology encompasses a quaternion-based hybrid attitude controller and a position controller that relies on nested saturation functions.

In this paper, an MRP-based hybrid backstepping control strategy is devised for trajectory tracking. First, a feedback law is designed with the intent of globally asymptotically stabilize the position error dynamics. The feedback regards saturation to bypass the singularities caused by non-positive thrust values. Afterward, an MRP-based hybrid backstepping controller encapsulating the saturated position feedback law is designed for the full dynamic system. The hybrid formulation provides a structure capable of capturing the MRP discontinuity. The MRPs have an inherent mechanism to drive the quadrotor automatically through the shortest rotational direction [3]. This characteristic prevents the unwinding phenomenon and constitutes an advantage compared to quaternion-based solutions, which require additional control states to guarantee this behavior. A second advantage stems from the MRP description only requiring three parameters to describe the attitude of a rigid-body instead of four, as in the quaternion case. The resulting control structure can track a position trajectory for any initial state while minimizing the distance to a reference rotation matrix and is robust to small measurement noise. Simulation results with a realistic model validate the strategy. To the authors' best knowledge, this solution is the first MRP-based hybrid strategy for quadrotor trajectory tracking.

This paper is organized as follows: the notation used and some preliminaries are presented in section II; the physical model is detailed and the control problem is formulated in section III; the saturated position tracking is addressed in section IV; the MRP-based hybrid backstepping controller for the full dynamic system is devised and the global asymptotic stability result is proved in section V; the simulation results obtained with the proposed solution are presented and discussed in section VI; lastly, some concluding remarks are drawn in section VII.

II. Notation and Preliminaries

$\mathbb{R}^n$ represents the n-dimensional Euclidean space; $\mathbb{R}_{\geq 0}$ expresses the set of non-negative real numbers; $\mathbb{N}$ symbolizes the set of natural numbers; $K\mathbb{B}^n$ denotes the closed ball of radius K centered at the origin of $\mathbb{R}^n$; $\mathbb{R}^{n\times m}$ denotes the set of $n\times m$ matrices; $\mathbb{S}^n = \left\{\mathbf{x}\in\mathbb{R}^{n+1} : \mathbf{x}^\top\mathbf{x} = 1\right\}$ symbolizes the n-dimensional unit sphere; $\mathbf{F}:\mathcal{X}\rightrightarrows\mathcal{Y}$ represents the set-valued map $\mathbf{F}$ from $\mathcal{X}$ to $\mathcal{Y}$; $\bar{\mathbf{C}}$ denotes the closure of the set $\mathbf{C}$; dom V symbolizes the domain of the function V; $V^{-1}(\mu)$ expresses the μ-level set of the function V, which is the set of points $\{x\in \mathrm{dom}V : V(x) = \mu\}$; $\mathbf{I_n}\in\mathbb{R}^{n\times n}$ represents the n-dimensional identity matrix; $\mathbf{e_i}\in\mathbb{R}^3$ denotes a vector of zeros except for the i$^{\text{th}}$ entry which is 1; $\|\cdot\|$ represents the Euclidean norm, $[\boldsymbol{\omega}]_\times$ is such that $[\boldsymbol{\omega}]_\times \mathbf{s} = \boldsymbol{\omega}\times\mathbf{s}$ for each $\mathbf{s},\boldsymbol{\omega}\in\mathbb{R}^3$, where $\times$ denotes the cross product; $\mathrm{Tr}(\cdot)$ symbolizes the trace of a given square matrix. The saturation functions considered in this work are aligned with the following definition:

Definition 1: The mapping $\boldsymbol{\sigma}:\mathbb{R}^m\mapsto\mathbb{R}^m$ is an independent symmetric function, i.e., $\boldsymbol{\sigma}(\mathbf{s}) \triangleq [\sigma_1(s_1)\cdots\sigma_m(s_m)]$ where each σ_i is a smooth non-decreasing function satisfying the following properties: (1) $\sigma_i(0) = 0$; (2) $s_i\sigma_i(s_i) > 0\ \forall\ s_i\neq 0$; (3) $\lim_{s_i\to\pm\infty}\sigma_i(s_i) = \pm M$, with $M>0$. ■

Concerning rigid-body attitude description, $\mathbf{R}$ represents an element of the three dimensional special orthogonal SO(3) and $\mathbf{q}\in\mathbb{S}^3$ denotes the unit quaternion and is defined by the pair $(q_0,\mathbf{q_1})$, where $q_0\in\mathbb{R}$ and $\mathbf{q_1}\in\mathbb{R}^3$ correspond, respectively, to the scalar and vector components. In addition to the previous representations, the MRP vector, $\boldsymbol{\vartheta}\in\mathbb{R}^3$, can also be used to parameterize the attitude. Each $\boldsymbol{\vartheta}$ has a shadow MRP associated, $\boldsymbol{\vartheta}^s\in\mathbb{R}^3$. Both $\boldsymbol{\vartheta}$ and $\boldsymbol{\vartheta}^s$ are related to a given unit quaternion through

$$\boldsymbol{\vartheta} = \mathbf{q_1}(1+q_0)^{-1} \tag{1a}$$

$$\boldsymbol{\vartheta}^s = -\mathbf{q_1}(1-q_0)^{-1} \tag{1b}$$

The shadow set can be obtained from the original set by resorting to the map $\boldsymbol{\Upsilon}:\mathbb{R}^3\setminus\{\mathbf{0}\}\mapsto\mathbb{R}^3$:

$$\boldsymbol{\vartheta^s} = \boldsymbol{\Upsilon}(\boldsymbol{\vartheta}) = -\boldsymbol{\vartheta}\|\boldsymbol{\vartheta}\|^{-2} \tag{2}$$

Both the original and the shadow MRP respect the following kinematic equation [3]

$$\dot{\boldsymbol{\vartheta}} = \mathbf{T}(\boldsymbol{\vartheta})\boldsymbol{\omega} = \frac{1}{4}\left((1-\|\boldsymbol{\vartheta}\|^2)\mathbf{I_3} + 2\,[\boldsymbol{\vartheta}]_\times + 2\boldsymbol{\vartheta}\boldsymbol{\vartheta}^\top\right)\boldsymbol{\omega} \tag{3}$$

The mapping $\mathbf{R}(\boldsymbol{\vartheta}):\mathbb{R}^3\mapsto$ SO(3)

$$\mathbf{R}(\boldsymbol{\vartheta}) := \mathbf{I_3} + \frac{4\left(2\,[\boldsymbol{\vartheta}]_\times^2 - (1-\|\boldsymbol{\vartheta}\|^2)\,[\boldsymbol{\vartheta}]_\times\right)}{(1+\|\boldsymbol{\vartheta}\|^2)^2} \tag{4}$$

maps a given $\boldsymbol{\vartheta}$ to a rotation matrix. For further details regarding MRP, the reader is referred to [3].

A hybrid system $\mathcal{H}$ is characterized by the data ($\mathbf{C}$, $\mathbf{F}$, $\mathbf{D}$, $\mathbf{G}$) and its model can be represented in the following form

$$\mathcal{H}\begin{cases}\dot{\mathbf{x}}\in\mathbf{F}(\mathbf{x}) & ,\quad \mathbf{x}\in\mathbf{C}\\ \mathbf{x}^+\in\mathbf{G}(\mathbf{x}) & ,\quad \mathbf{x}^+\in\mathbf{D}\end{cases} \tag{5}$$

The hybrid system evolves according to the set-valued map $\mathbf{F}:\mathbb{R}^n\rightrightarrows\mathbb{R}^n$ while in the flow set $\mathbf{C}\subset\mathbb{R}^n$ and instantaneously changes under the set-valued map $\mathbf{G}:\mathbb{R}^n\rightrightarrows\mathbb{R}^n$ while in the jump set $\mathbf{D}\subset\mathbb{R}^n$. A solution $\mathbf{x}(t,j)$ to $\mathcal{H}$, with t and j denoting, respectively, ordinary time and jump time, is a function $\mathbf{x}:\mathrm{dom}\,\mathbf{x}\mapsto\mathbb{R}^n$, where $\mathrm{dom}\,\mathbf{x}\subset\mathbb{R}_{\geq 0}\times\mathbb{N}$ is a hybrid time domain. For further details, see [12], [13].

III. Problem Formulation

In this paper, a controller for quadrotors is designed envisioning a global trajectory tracking capacity. To this end, the dynamics of these vehicles are considered to be governed by the following set of differential equations [14]:

$$\dot{\mathbf{p}} = \mathbf{v},\quad \dot{\mathbf{v}} = -g\mathbf{e_3} + \mathbf{R}\mathbf{e_3}\frac{T}{m} \tag{6a}$$

$$\dot{\mathbf{R}} = \mathbf{R}\,[\boldsymbol{\omega}]_\times,\quad \mathbf{J}\dot{\boldsymbol{\omega}} = \mathbf{J}\boldsymbol{\omega}\times\boldsymbol{\omega} + \boldsymbol{\tau} \tag{6b}$$

where $\mathbf{p}\in\mathbb{R}^3$ represents the position of the aerial vehicle in the inertial frame, $\mathbf{v}\in\mathbb{R}^3$ denotes the velocity in the inertial frame, $\mathbf{a}\in\mathbb{R}^3$ symbolizes the acceleration in the inertial frame, $g\in\mathbb{R}$ corresponds to the gravity acceleration, $T\in\mathbb{R}$ symbolizes the thrust magnitude, $\mathbf{R}\in$ SO(3) is the rotation matrix from the body-fixed to the inertial frame, $m\in\mathbb{R}$ is the total mass of the quadrotor, $\boldsymbol{\omega}\in\mathbb{R}^3$ represents the angular velocity expressed in the body-fixed frame, $\boldsymbol{\tau}\in\mathbb{R}^3$ represents the moment, and $\mathbf{J}\in\mathbb{R}^{3\times 3}$ corresponds to the quadrotor diagonal tensor of inertia.

Following a control problem construction similar to [9], let the desired trajectory be defined, for $t\geq 0$, by the map

$$\mathbf{r}(t) := \left(\mathbf{p_d}(t), \dot{\mathbf{p}}_\mathbf{d}(t), \ddot{\mathbf{p}}_\mathbf{d}(t), \mathbf{p_d^{(3)}}(t), \mathbf{R_r}(t), \boldsymbol{\omega}_\mathbf{d}(t)\right), \tag{7}$$

which encompasses the desired position, $\mathbf{p_d}$, and attitude, $\mathbf{R_r}$, and the respective derivatives. In addition, let the trajectory $\mathbf{r}(t)$ verify the conditions detailed in Assumption 1.

Assumption 1: The reference trajectory $\mathbf{r}(t)$ is characterized by the following system:

$$\begin{cases}\dot{\mathbf{r}}\in\mathbf{F_r}(\mathbf{r}) := \left(\dot{\mathbf{p}}_\mathbf{d}, \ddot{\mathbf{p}}_\mathbf{d}, \mathbf{p_d^{(3)}}, K_p\mathbb{B}^3, \mathbf{R_r}[\omega_\mathbf{d}]_\times, K_{\dot{\omega}}\mathbb{B}^3\right)\\ \mathbf{r}\in\boldsymbol{\Omega}\subset\mathbb{R}^3\times\mathbb{R}^3\times\mathbb{R}^3\times\mathbb{R}^3\times\mathrm{SO(3)}\times\mathbb{R}^3\end{cases} \tag{8}$$

where $\boldsymbol{\Omega}$ satisfies $\mathbf{e}_3^\top\mathbf{R_r}(t)\mathbf{e}_3\geq 0\ \ \forall\ \ t\geq 0$ and is compact. Furthermore, the desired acceleration $\ddot{\mathbf{p}}_\mathbf{d}(t)$ is bounded by

$$\sup_{\mathbf{r}\,\in\,\boldsymbol{\Omega}}\|\ddot{\mathbf{p}}_\mathbf{d}(t)\| < g - \sqrt{3}\,(M_p + M_v)\,,\quad\forall\ \ t\geq 0 \tag{9}$$

where M_p and M_v are saturation levels to be defined during the controller design. ■

The quadrotor, since it is an underactuated vehicle, is unable to perform an arbitrary trajectory. In this regard, to prevent a scenario of incompatibility between the desired rotation matrix $\mathbf{R_r}$ and the thrust direction imposed by the position tracking, the following optimization problem [5]

$$\begin{aligned} \mathbf{R_d} \;=\; & \arg\min_{\mathbf{R}} \;\; \frac{1}{2}\,\mathrm{Tr}\left(\mathbf{I_3} - \mathbf{R}\mathbf{R_r^{-1}}\right) \\ & \text{s.t.} \qquad \mathbf{R}\mathbf{e_3} = \boldsymbol{\alpha} \end{aligned} \tag{10}$$

where $\boldsymbol{\alpha} \in \mathbb{B}^3$ denotes the thrust direction obtained from the position control, is resorted to. Solving this problem is equivalent to finding the "closest" feasible rotation matrix, $\mathbf{R_d} \in$ SO(3), in the sense of the cost function, that verifies the condition imposed by the position tracking subsystem, $\mathbf{R_d}\mathbf{e_3} = \boldsymbol{\alpha}$. To this end, the degree of freedom associated with the rotation around the vector $\boldsymbol{\alpha}$ is exploited. In this way, the control problem can be stated as follows:

Problem 1: Design $T \in \mathbb{R}_{>0}$ and $\boldsymbol{\tau} \in \mathbb{R}^3$ to globally asymptotically stabilize the set

$$\mathcal{A} = \{(\mathbf{r}, \mathbf{x}) \in \boldsymbol{\Omega} \times \boldsymbol{\chi} : \mathbf{p} = \mathbf{p_d}, \, \mathbf{R} = \mathbf{R_d}\} \tag{11}$$

with $\mathbf{x} := (\mathbf{p}, \mathbf{v}, \mathbf{R}, \boldsymbol{\omega}) \in \boldsymbol{\chi} := \mathbb{R}^3 \times \mathbb{R}^3 \times$ SO(3) $\times \mathbb{R}^3$, for the closed-loop system that results from the application of the designed control law to the system (6). ■

IV. SATURATED POSITION TRACKING

Let the position and velocity tracking errors be defined by

$$\tilde{\mathbf{p}} = \mathbf{p} - \mathbf{p_d}, \quad \tilde{\mathbf{v}} = \mathbf{v} - \dot{\mathbf{p}}_\mathbf{d} \tag{12}$$

From (6a), the error dynamics can be expressed as follows:

$$\dot{\tilde{\mathbf{p}}} = \tilde{\mathbf{v}}, \quad \dot{\tilde{\mathbf{v}}} = -g\mathbf{e_3} + \mathbf{R}\mathbf{e_3}\frac{T}{m} - \ddot{\mathbf{p}}_\mathbf{d} \tag{13}$$

It is intended to obtain from the position control the magnitude and direction of the thrust force required to perform the desired trajectory $\mathbf{r}(t)$. To this end, the rotation matrix $\mathbf{R}$ and the thrust force T are considered inputs and a control vector $\mathbf{u_p} \in \mathbb{R}^3 \setminus \{\mathbf{0}\}$ satisfying

$$\mathbf{u_p} := \mathbf{R}\mathbf{e_3}\frac{T}{m} \tag{14}$$

is designed. In this way, the thrust input can be computed through

$$T := m\|\mathbf{u_p}\| \tag{15}$$

As stated in Problem 1, the control law has to generate only positive values for thrust T. This can be accomplished by resorting to a controller that explicitly addresses saturation (see [15], [16]). Hence, the saturated feedback control law

$$\mathbf{u_p} := -\boldsymbol{\sigma_p}\left(k_p\left(\tilde{\mathbf{p}} + \tilde{\mathbf{v}}\right)\right) - \boldsymbol{\sigma_v}\left(k_v\tilde{\mathbf{v}}\right) + g\mathbf{e}_3 + \ddot{\mathbf{p}}_\mathbf{d}, \tag{16}$$

with $k_p > 0$, $0 < k_v < 4$ (this bound will become clear next), and where $\boldsymbol{\sigma_p}$ and $\boldsymbol{\sigma_v}$ are saturation functions, verifying the properties detailed in Definition 1, with M_p and M_v as saturation levels, respectively. With the control law (16), the error dynamics reshape into:

$$\dot{\tilde{\mathbf{x}}}_\mathbf{p} = \mathbf{F_p}\left(\mathbf{r}, \tilde{\mathbf{x}}_\mathbf{p}\right) := \begin{pmatrix} \tilde{\mathbf{v}} \\ -\boldsymbol{\sigma_p}\left(k_p\left(\tilde{\mathbf{p}} + \tilde{\mathbf{v}}\right)\right) - \boldsymbol{\sigma_v}\left(k_v\tilde{\mathbf{v}}\right) \end{pmatrix} \tag{17}$$

where $\tilde{\mathbf{x}}_\mathbf{p} := (\tilde{\mathbf{p}}, \tilde{\mathbf{v}})$ belongs to $\boldsymbol{\chi}_\mathbf{p} := \mathbb{R}^3 \times \mathbb{R}^3$.

Theorem 1: Let the conditions expressed in Assumption 1 hold for all $t \geq 0$. Then, the set

$$\mathcal{A}_p = \left\{\tilde{\mathbf{x}}_\mathbf{p} \in \boldsymbol{\chi}_\mathbf{p} : \tilde{\mathbf{p}} = \mathbf{0}, \; \tilde{\mathbf{v}} = \mathbf{0}\right\} \tag{18}$$

is globally uniformly asymptotically stable for the system (17). Moreover, the thrust T resulting from the control law is upper and lower bounded as follows

$$0 < T < 2mg \tag{19}$$

for each solution $\tilde{\mathbf{x}}_\mathbf{p}(t)$ defined for $t \geq 0$.

Proof: Consider the error dynamics detailed in (17) and let $V_1 : \boldsymbol{\chi}_\mathbf{p} \mapsto \mathbb{R}_{\geq 0}$ be a Lyapunov candidate function defined by

$$V_1\left(\tilde{\mathbf{x}}_\mathbf{p}\right) := \sum_{i=1}^{3}\left(\frac{k_p}{2}\left(\mathbf{e}_i^\top\tilde{\mathbf{v}}\right)^2 + \int_0^{k_p\mathbf{e}_i^\top(\tilde{\mathbf{p}}+\tilde{\mathbf{v}})}\sigma_{p_i}\left(\mu\right)\,d\mu\right) \tag{20}$$

The Lyapunov function V_1 is continuous, radially unbounded, and positive-definite with respect to the set $\mathcal{A}_p$. The time derivative of V_1 is given by

$$\begin{aligned} \dot{V}_1 = &- k_p\left(\|\boldsymbol{\sigma_p}\left(k_p\left(\tilde{\mathbf{p}} + \tilde{\mathbf{v}}\right)\right)\|^2 + \tilde{\mathbf{v}}^\top\boldsymbol{\sigma_v}\left(k_v\tilde{\mathbf{v}}\right)\right) \\ &- k_p\left(\boldsymbol{\sigma_p}\left(k_p\left(\tilde{\mathbf{p}} + \tilde{\mathbf{v}}\right)\right)^\top\boldsymbol{\sigma_v}\left(k_v\tilde{\mathbf{v}}\right)\right), \end{aligned} \tag{21}$$

which yields

$$\dot{V}_1 \leq -k_p\boldsymbol{\beta}^\top\begin{bmatrix} \mathbf{I_3} & \frac{1}{2}\mathbf{I_3} \\ \frac{1}{2}\mathbf{I_3} & \frac{1}{k_v}\mathbf{I_3} \end{bmatrix}\boldsymbol{\beta} = -\mathbf{W}(\tilde{\mathbf{x}}_\mathbf{p}) \leq 0 \tag{22}$$

with $\boldsymbol{\beta} := \left(\boldsymbol{\sigma_p}\left(k_p\left(\tilde{\mathbf{p}} + \tilde{\mathbf{v}}\right)\right), \boldsymbol{\sigma_v}\left(k_v\tilde{\mathbf{v}}\right)\right)$ and $\mathbf{W}(\tilde{\mathbf{x}}_\mathbf{p})$ is a continuous positive-definite function on $\boldsymbol{\chi}_\mathbf{p}$. Thus, $\dot{V}_1$ is negative definite with respect to the set $\mathcal{A}_p$. From [17, Theorem 4.9], the set $\mathcal{A}_p$ is globally uniformly asymptotically stable for the system (17). Concerning the bounds of T, the norm of the control law (16) is given by

$$\|\mathbf{u_p}\| = \| - \boldsymbol{\sigma_p}\left(k_p\left(\tilde{\mathbf{p}} + \tilde{\mathbf{v}}\right)\right) - \boldsymbol{\sigma_v}\left(k_v\tilde{\mathbf{v}}\right) + g\mathbf{e}_3 + \ddot{\mathbf{p}}_\mathbf{d}\|, \tag{23}$$

Applying the triangle inequality and recalling the properties detailed in Definition 1, the acceleration condition expressed in Assumption 1, and (15), yields the upper bound $T < 2mg$. If the reverse triangle inequality is applied instead, the lower bound $T > 0$ is achieved. Thus, for each solution $\tilde{\mathbf{x}}_\mathbf{p}(t)$ defined for $t \geq 0$, the thrust T satisfies $0 < T < 2mg$. ■

V. GLOBAL ASYMPTOTIC TRACKING FOR THE FULL SYSTEM

The position controller designed in section IV dictates the magnitude and direction of the thrust force required to track the trajectory. By recalling (14), let $\boldsymbol{\alpha} \in \mathbb{B}^3$ denote the thrust direction resulting from the position control

$$\boldsymbol{\alpha}\left(\mathbf{u_p}\right) := \mathbf{u_p}\|\mathbf{u_p}\|^{-1} \tag{24}$$

In this way, the constraint of (10) is defined. The minimization problem (10) has an unique solution [5]. Given the condition $\mathbf{e}_3^\top\mathbf{R_r}(t)\mathbf{e}_3 \geq 0 \;\forall\; t \geq 0$ and (9), one has $\mathbf{e}_3^\top\mathbf{R}_\mathbf{r}^\top\mathbf{u_p} \neq -\|\mathbf{u_p}\| \;\forall\, t \geq 0$. Then, it follows from [9] that the solution is obtained through

$$\mathbf{R_d} = \mathbf{B}\left(\boldsymbol{\alpha}, \boldsymbol{\zeta}, \mathbf{R_r}\right)\mathbf{R_r} \tag{25}$$

where $\boldsymbol{\zeta} \in \mathbb{R}^3$ is defined by $\boldsymbol{\zeta} := [\mathbf{R_r}\mathbf{e}_3]_\times \boldsymbol{\alpha}$ and $\mathbf{B}(\boldsymbol{\alpha}, \boldsymbol{\zeta}, \mathbf{R_r})$ results from the following formula:

$$\mathbf{B}(\boldsymbol{\alpha}, \boldsymbol{\zeta}, \mathbf{R_r}) = \mathbf{I_3} + [\zeta]_\times + \left(1 + \mathbf{e}_3^\top \mathbf{R_r}^\top \boldsymbol{\alpha}\right)^{-1} [\boldsymbol{\zeta}]_\times^2 \quad (26)$$

In addition to $\mathbf{R_d}$, the angular velocity and acceleration references can be obtained from $\mathbf{u_p}$ as well. Computing the time derivative of the desired thrust direction yields

$$\frac{d(\mathbf{R_d e_3})}{dt} = \left(\mathbf{I_3} - \frac{\mathbf{u_p u_p}^\top}{\|\mathbf{u_p}\|^2}\right) \frac{\dot{\mathbf{u}}_\mathbf{p}}{\|\mathbf{u_p}\|} \quad (27)$$

Combining with the kinematic equation in (6b) leads to

$$[\boldsymbol{\omega}_\mathbf{d}]_\times \mathbf{e_3} = \mathbf{R_d}^\top \left(\mathbf{I_3} - \frac{\mathbf{u_p u_p}^\top}{\|\mathbf{u_p}\|^2}\right) \frac{\dot{\mathbf{u}}_\mathbf{p}}{\|\mathbf{u_p}\|} \quad (28)$$

The former expression enables determining the desired angular velocities $\mathbf{e_1}^\top \boldsymbol{\omega}_\mathbf{d}$ and $\mathbf{e_2}^\top \boldsymbol{\omega}_\mathbf{d}$. Regarding the third component of $\boldsymbol{\omega}_\mathbf{d}$, since the thrust direction does not constraint the rotation around itself, this reference is defined by the user in accordance with $\mathbf{R_r}$. Differentiating with respect to time both sides of (28) yields

$$[\dot{\boldsymbol{\omega}}_\mathbf{d}]_\times \mathbf{e_3} = -[\boldsymbol{\omega}_\mathbf{d}]_\times \mathbf{R_d}^\top \frac{d(\mathbf{R_d e_3})}{dt} + \mathbf{R_d}^\top \frac{d^2(\mathbf{R_d e_3})}{dt} \quad (29)$$

with

$$\begin{aligned}\frac{d^2(\mathbf{R_d e_3})}{dt} = & \frac{\ddot{\mathbf{u}}_\mathbf{p}\|\mathbf{u_p}\|^2 - 2\dot{\mathbf{u}}_\mathbf{p}\mathbf{u_p}^\top\dot{\mathbf{u}}_\mathbf{p} - \mathbf{u_p}\|\dot{\mathbf{u}}_\mathbf{p}\|^2}{\|\mathbf{u_p}\|^3} \\ & - \frac{\mathbf{u_p u_p}^\top \ddot{\mathbf{u}}_\mathbf{p}}{\|\mathbf{u_p}\|^3} + \frac{3\mathbf{u_p u_p}^\top \dot{\mathbf{u}}_\mathbf{p} \dot{\mathbf{u}}_\mathbf{p}^\top \mathbf{u_p}}{\|\mathbf{u_p}\|^5}\end{aligned} \quad (30)$$

From (29), the desired angular acceleration $\mathbf{e_1}^\top \dot{\boldsymbol{\omega}}_\mathbf{d}$ and $\mathbf{e_2}^\top \dot{\boldsymbol{\omega}}_\mathbf{d}$ are defined. The desired angular acceleration $\mathbf{e_3}^\top \dot{\boldsymbol{\omega}}_\mathbf{d}$ results from the user-defined angular velocity $\mathbf{e_3}^\top \boldsymbol{\omega}_\mathbf{d}$.

As formerly discussed, the modified Rodrigues parameters can be resorted to parameterize the attitude. Let $\tilde{\mathbf{R}} \in \mathrm{SO}(3)$ denote the rotation matrix error given by $\tilde{\mathbf{R}} = \mathbf{R}\mathbf{R_d}^\top$ and that satisfies $\mathbf{R}(\tilde{\boldsymbol{\vartheta}}) = \tilde{\mathbf{R}}$. The MRP error $\tilde{\boldsymbol{\vartheta}} \in \mathbb{R}^3$ satisfies the kinematic equation

$$\dot{\tilde{\boldsymbol{\vartheta}}} = \mathbf{T}(\tilde{\boldsymbol{\vartheta}})(\boldsymbol{\omega} - \mathbf{R}(\tilde{\boldsymbol{\vartheta}})^\top \boldsymbol{\omega}_\mathbf{d}) \quad (31)$$

with $\mathbf{R}(\tilde{\boldsymbol{\vartheta}}) = \tilde{\mathbf{R}}$. To compute $\tilde{\boldsymbol{\vartheta}}$ from $\mathbf{R}(\tilde{\boldsymbol{\vartheta}})$, first, the hybrid-dynamic path-lifting algorithm proposed in [10] is applied to uniquely convert the rotation matrix error into its unit quaternion representation $\tilde{\mathbf{q}} \in \mathbb{S}^3$. Then, using (1), the MRP error $\tilde{\boldsymbol{\vartheta}}$ is computed from the unit quaternion depending on its scalar part $\tilde{q}_0$: if $\tilde{q}_0 \geq 0$, (1a) is used; otherwise, (1b) is used instead. As such, the bound $\|\tilde{\boldsymbol{\vartheta}}\| \leq 1$, corresponding to the error associated with the shortest rotation, is guaranteed [3, p. 120]. This equivalence enables dealing effectively with tumbling situations, namely when the quadrotor has performed a principal rotation beyond $\pm 180°$ away from the angular reference. In practical terms, this translates into the quadrotor completing the revolution instead of attempting to force it back. Hence, this MRP property allows avoiding the *unwinding phenomenon* without requiring additional control mechanisms (cf. [1]).

A hybrid control methodology relying on backstepping was devised considering the position control designed in section IV. Resorting to this nonlinear control method enables canceling the effects of the attitude error on the position dynamics. Let $\tilde{\boldsymbol{\omega}} \in \mathbb{R}^3$ be given by $\tilde{\boldsymbol{\omega}} := \boldsymbol{\omega} - \boldsymbol{\omega}^*$, where $\boldsymbol{\omega}^*$ is a virtual controller satisfying

$$\boldsymbol{\omega}^* := -k_\vartheta \tilde{\boldsymbol{\vartheta}} + \tilde{\mathbf{R}}^\top \boldsymbol{\omega}_\mathbf{d} - k_b \boldsymbol{\varsigma} \quad (32)$$

with $k_\vartheta, k_b > 0$ and

$$\boldsymbol{\varsigma} := \left(\frac{-8[\tilde{\boldsymbol{\vartheta}}]_\times [\mathbf{u_p}]_\times + 4(1 - \|\tilde{\boldsymbol{\vartheta}}\|^2)[\mathbf{u_p}]_\times}{(1 + \|\tilde{\boldsymbol{\vartheta}}\|^2)^2}\right)^\top \frac{\partial V_1}{\partial \tilde{\mathbf{v}}}. \quad (33)$$

The vector $\boldsymbol{\varsigma}$ serves the purpose of canceling the interconnection term of the position dynamics, $(\tilde{\mathbf{R}} - \mathbf{I})\mathbf{u_p}$, caused by the attitude error. Let the feedback law $\boldsymbol{\tau}$ be defined as follows

$$\boldsymbol{\tau} = -k_\omega \tilde{\boldsymbol{\omega}} - \tilde{\boldsymbol{\vartheta}} - [\mathbf{J}\boldsymbol{\omega}]_\times \boldsymbol{\omega} + \mathbf{J}\dot{\boldsymbol{\omega}}^*. \quad (34)$$

with $k_\omega > 0$. The hybrid framework provides a structure capable of capturing the switches between the original and the shadow MRP error representations and the resulting effects. Let $\mathbf{x_h} := (\mathbf{r}, \tilde{\mathbf{x}}_\mathbf{p}, \tilde{\boldsymbol{\vartheta}}, \tilde{\boldsymbol{\omega}}) \in \boldsymbol{\chi}_1$, with $\boldsymbol{\chi}_1 = \boldsymbol{\Omega} \times \boldsymbol{\chi}_\mathbf{p} \times \mathbb{R}^3 \times \mathbb{R}^3$ in furtherance of formalizing the hybrid $\mathcal{H} = (\mathbf{C}, \mathbf{F}, \mathbf{D}, \mathbf{G})$:

$$\mathbf{F}(\mathbf{x_h}) := \begin{pmatrix} \mathbf{F_r}(r) \\ \tilde{\mathbf{v}} \\ \tilde{\mathbf{R}}\mathbf{R_d e_3}\|\mathbf{u_p}\| - g\mathbf{e_3} - \ddot{\mathbf{p}}_\mathbf{d} + \mathbf{b} \\ \mathbf{T}(\tilde{\boldsymbol{\vartheta}})\left(\boldsymbol{\omega} - \mathbf{R}(\tilde{\boldsymbol{\vartheta}})^\top \boldsymbol{\omega}_\mathbf{d}\right) \\ \mathbf{J}^{-1}\left([\mathbf{J}\boldsymbol{\omega}]_\times \boldsymbol{\omega} + \boldsymbol{\tau}\right) - \dot{\boldsymbol{\omega}}^* \end{pmatrix} \quad (35a)$$

$$\mathbf{C} := \left\{\mathbf{x_h} \in \boldsymbol{\chi}_1 : \|\tilde{\boldsymbol{\vartheta}}\| \leq 1 + \delta\right\} \quad (35b)$$

$$\mathbf{G}(\mathbf{x_h}) := (\mathbf{r}, \tilde{\mathbf{x}}_\mathbf{p}, \boldsymbol{\Upsilon}(\tilde{\boldsymbol{\vartheta}}), \tilde{\boldsymbol{\omega}}) \quad (35c)$$

$$\mathbf{D} := \left\{\mathbf{x_h} \in \boldsymbol{\chi}_1 : \|\tilde{\boldsymbol{\vartheta}}\| \geq 1 + \delta\right\} \quad (35d)$$

for some $\delta > 0$ and with $\boldsymbol{\tau}$ satisfying (34). With the inclusion of the parameter δ, the switching between the original and shadow sets becomes hysteretic. In this way, assuming the measurements are corrupted by a upper-bounded noise, by setting the hysteresis parameter δ to a greater value, noise-induced chattering is avoided [4]. Therefore, the switch becomes robust to measurement noise. In Lemma 1, it is shown that the hybrid system $\mathcal{H}$ fulfils the hybrid basic conditions stated in [12].

Lemma 1: The hybrid system $\mathcal{H}$, described in (35), verifies the hybrid basic conditions.

Proof: The flow set $\mathbf{C}$ is closed and the map $\boldsymbol{\Upsilon}$ is continuous on $\mathbf{D}$. Consequently, since the inverse image of a closed set under a continuous mapping is closed, the jump set $\mathbf{D}$ is closed. The flow map $\mathbf{F}$ is a single-valued mapping. The mappings $K_p\mathbb{B}^3$ and $K_{\dot{\omega}}\mathbb{B}^3$ are convex and bounded. Furthermore, since both are independent of $\mathbf{x_h}$, the respective graphs are closed and, therefore, outer semicontinuous. The remaining functions that $\mathbf{F}$ encompasses are continuous on $\mathbf{C}$, thus, are outer semicontinuous and locally bounded, and correspond to differential equations, which, according to [13, Assumption 6.5], can be identified with a hybrid system satisfying hybrid basic conditions. Since the single-valued mapping $\boldsymbol{\Upsilon}$ is continuous and $\boldsymbol{\Upsilon}(\tilde{\boldsymbol{\vartheta}})$ yields $\|\tilde{\boldsymbol{\vartheta}}\| \leq (1+\delta)^{-1}$ for $\mathbf{x_h} \in \mathbf{D}$, and $\tilde{\boldsymbol{\omega}}$, $\mathbf{r}$, and $\tilde{\mathbf{x}}_\mathbf{p}$ remain constant during jumps, $\mathbf{D} \times \mathbf{G}(\mathbf{D})$ is closed and $\mathbf{G}(\mathbf{D})$ is bounded. Hence, $\mathbf{G}$ is outer semicontinuous [13, Lemma 5.10] and locally bounded [13, Definition 5.14] relative to $\mathbf{D}$. ■

In Theorem 2, the global asymptotic stability result for the compact set $\mathcal{A}_1 := \left\{\mathbf{x_h} \in \chi_1 : \tilde{\mathbf{x}}_\mathbf{p} \in \mathcal{A}_p,\, \tilde{\boldsymbol{\vartheta}} = \mathbf{0},\, \tilde{\boldsymbol{\omega}} = \mathbf{0}\right\}$ is proved.

Theorem 2: The solutions of the closed-loop hybrid system (35) are complete and bounded, and the compact set $\mathcal{A}_1$ is globally asymptotically stable for $\mathcal{H}$.

Proof: Let $V_2(\mathbf{x_h}) : \boldsymbol{\chi}_1 \mapsto \mathbb{R}_{\geq 0}$ be a function given by

$$V_2(\mathbf{x_h}) = k_b V_1 + 2\ln\left(1 + \tilde{\boldsymbol{\vartheta}}^\top \tilde{\boldsymbol{\vartheta}}\right) + \frac{1}{2}\tilde{\boldsymbol{\omega}}^\top \mathbf{J}\tilde{\boldsymbol{\omega}}, \tag{36}$$

The function V_2 is continuously differentiable on $\boldsymbol{\chi}_1$ and radially unbounded. Hence, since, from Assumption 1, $\mathbf{r}$ belongs to a compact set, the sublevel sets of V_2 are compact. In particular, for any initial condition $\mathbf{x_h}(0,0)$, the set $\mathbf{U} = \{\mathbf{x_h} \in \boldsymbol{\chi}_1 : V_2(\mathbf{x_h}) \leq V_2(\mathbf{x_h}(0,0))\}$ is compact. Computing the time derivative of V_2 yields

$$\dot{V}_2 \leq -\mathbf{W}(\tilde{\mathbf{x}}_\mathbf{p}) - k_{\boldsymbol{\vartheta}}\tilde{\boldsymbol{\vartheta}}^\top\tilde{\boldsymbol{\vartheta}} - k_{\boldsymbol{\omega}}\tilde{\boldsymbol{\omega}}^\top\tilde{\boldsymbol{\omega}} \tag{37}$$

Note that the property $4\tilde{\boldsymbol{\vartheta}}^\top \mathbf{T}(\tilde{\boldsymbol{\vartheta}}) = (1+\tilde{\boldsymbol{\vartheta}}^\top\tilde{\boldsymbol{\vartheta}})\tilde{\boldsymbol{\vartheta}}^\top$, stated in [3, p. 123], was used. From (22) and (37), one concludes that $\dot{V}_2 \leq 0 \;\forall\; \mathbf{x_h} \in \mathbf{C}$. The behaviour of V_2 during jumps is characterized by

$$V_2(\mathbf{G}(\mathbf{x_h})) - V_2(\mathbf{x_h}) = 2\ln\left(\|\tilde{\boldsymbol{\vartheta}}\|^{-2}\right) \tag{38}$$

Since for $\mathbf{x_h} \in \mathbf{D}$ one has $\|\tilde{\boldsymbol{\vartheta}}\| \geq 1+\delta$, the previous expression yields

$$V_2(\mathbf{G}(\mathbf{x_h})) - V_2(\mathbf{x_h}) \leq -4\ln(1+\delta) < 0 \tag{39}$$

Hence, V_2 is monotonically decreasing along flows and strictly decreasing during jumps, which implies that any solution $\mathbf{x_h}(t,\, j)$ to $\mathcal{H}$ remains in $\mathbf{U}$ for all $(t,j) \in \operatorname{dom} \mathbf{x_h}$. Moreover, in the view of $\mathbf{G}(\mathbf{D}) \subset \mathbf{C}$, it can be concluded that the maximal solutions of $\mathcal{H}$ do not jump out of $\mathbf{C} \cup \mathbf{D}$. Therefore, each maximal solution to $\mathcal{H}$ is bounded and complete [12, Theorem S3].

Consider the functions

$$u_c(\mathbf{x_h}) = \begin{cases} -\mathbf{W}(\tilde{\mathbf{p}},\tilde{\mathbf{v}}) - k_{\boldsymbol{\vartheta}}\tilde{\boldsymbol{\vartheta}}^\top\tilde{\boldsymbol{\vartheta}} - k_{\boldsymbol{\omega}}\tilde{\boldsymbol{\omega}}^\top\tilde{\boldsymbol{\omega}} & ,\mathbf{x_h} \in \mathbf{C} \\ -\infty & ,\mathbf{x_h} \notin \mathbf{C} \end{cases} \tag{40}$$

$$u_d(\mathbf{x_h}) = \begin{cases} -4\ln(1+\delta) & ,\mathbf{x_h} \in \mathbf{D} \\ -\infty & ,\mathbf{x_h} \notin \mathbf{D} \end{cases} \tag{41}$$

Following the invariance principle stated by Goebel et al. in [13, Theorem 8.2.], since $\mathbf{x_h}(\operatorname{dom} \mathbf{x_h}) \subset \mathbf{U}$, $u_c(\mathbf{x_h}) \leq 0, u_d(\mathbf{x_h}) < 0 \;\forall\; \mathbf{x_h} \in \mathbf{U}$, and V_2 is continuously differentiable on $\boldsymbol{\chi}_1 \supset \mathbf{C}$, each maximal solution to $\mathcal{H}$ approach the largest weakly invariant subset of

$$V_2^{-1}(r) \cap \mathbf{U} \cap \left[\overline{u_c^{-1}(0)} \cup \left(u_d^{-1}(0) \cap \mathbf{G}\left(u_d^{-1}(0)\right)\right)\right] \tag{42}$$

for some $r \in V_2(\mathbf{U})$. From the results formerly presented,

$$\overline{u_c^{-1}(0)} = \mathcal{A}_1 \tag{43}$$

$$u_d^{-1}(0) \cap \mathbf{G}\left(u_d^{-1}(0)\right) = \emptyset \tag{44}$$

Hence, $\mathcal{A}_1$ is globally attractive. Furthermore, in combination with the previous statements, since V_2 is positive-definite with respect to the compact set $\mathcal{A}_1$, it follows from [13, Theorem 8.8.] that $\mathcal{A}_1$ is globally stable. As a result, $\mathcal{A}_1$ is globally asymptotically stable for $\mathcal{H}$. ■

Considering (4), for $\mathbf{x_h} \in \mathcal{A}_1$, $\tilde{\boldsymbol{\vartheta}} = \mathbf{0}$ implies $\mathbf{R}(\tilde{\boldsymbol{\vartheta}}) = \mathbf{I_3}$, which in turn implies $\mathbf{R} = \mathbf{R_d}$. Moreover, from (12), $\tilde{\mathbf{p}} = \mathbf{0}$ yields $\mathbf{p} = \mathbf{p_d}$. Thereby, the global asymptotic stability result of $\mathcal{A}_1$ for (35) translates into a global stability results of $\mathcal{A}$ for (6). Hence, with T and $\boldsymbol{\tau}$ given by, respectively, (15) and (34), the control objective stated in Problem 1 is achieved. Furthermore, from [13, Theorem 6.30], since $\mathcal{H}$ verifies the hybrid basic conditions, the hybrid system is well-posed. Therefore, according to [13, Theorem 7.21], the hybrid system (35) is robust to small measurement noise.

VI. Simulation Results

In furtherance of validating the control strategy, a trajectory tracking test was conducted in simulation. The model considered to this end, in addition to the underlying differential equations described in (6), includes noise disturbance and actuators dynamics modelled from sensory data acquired with an actual quadcopter. The values considered for the quadrotor mass and inertia were, respectively, $m = 0.460$kg and $\mathbf{J} = \text{diag}(2.24\times10^{-3}, 2.90\times10^{-3}, 5.30\times10^{-3})$, and the selected sampling time for the simulation was 0.01 seconds. For more details regarding the simulation model, the reader is referred to [18].

To study the potential of the proposed control strategy, the capacity to track the following trajectory was evaluated:

$$\mathbf{p_d}(t) = (2\cos(2\pi f t), 2\sin(2\pi f t), 2.5 - 2\cos(2\pi f_z t)) \tag{45}$$

$$\mathbf{R_r} = \begin{bmatrix} \cos\psi_d(t) & -\sin\psi_d(t) & 0 \\ \sin\psi_d(t) & \cos\psi_d(t) & 0 \\ 0 & 0 & 1 \end{bmatrix} \tag{46}$$

with $f = \frac{1}{20}$Hz, $f_z = \frac{1}{10}$Hz, and $\psi_d(t) = \frac{2\pi}{90}t$ rad. In addition, $\mathbf{e_3}^\top\boldsymbol{\omega}_\mathbf{d}$ and $\mathbf{e_3}^\top\dot{\boldsymbol{\omega}}_\mathbf{d}$ were specified with the values $\mathbf{e_3}^\top\boldsymbol{\omega}_\mathbf{d} = \frac{2\pi}{90}$ and $\mathbf{e_3}^\top\dot{\boldsymbol{\omega}}_\mathbf{d} = 0$. The function $\sigma(s) = M\tanh\left(\frac{s}{M}\right)$ satisfies the properties enunciated in Definition 1 and was the saturation function used. Regarding the control parameters, the values $k_p = 6, k_v = 3, k_\omega = 0.01, k_\vartheta = 100, k_b = 0.001, M_p = 1, M_v = 1, \delta = 0.06$ were defined. In this way, the reference trajectory verifies the conditions detailed in Assumption 1. It is important to stress that the attitude gains were defined aiming faster responses when compared to the position subsystem. To study the MRP logic on which the hybrid system is based, an initial yaw angle of $\frac{3\pi}{2}$ rad was set.

The results attained with the designed control solution are depicted in Fig. 1. This figure shows that the approach successfully tracked the trajectory.

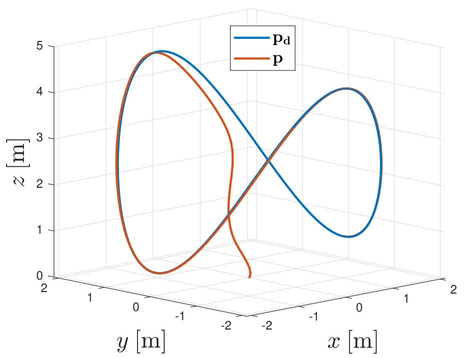

Fig. 1. Three dimensional graph of the response obtained for trajectory tracking in simulation.

In Fig. 2, the position and MRP error norm are presented. It is clear that both norms converge to zero, which attest the success in tracking the desired trajectory. Moreover, since the MRP error norm obtained verifies the flow set condition, to track the initial yaw angle reference, the quadrotor performed the smaller principal rotation, corresponding to the direction from $\frac{3\pi}{2} - 2\pi$ to 0. Hence, the MRP logic was successfully implemented.

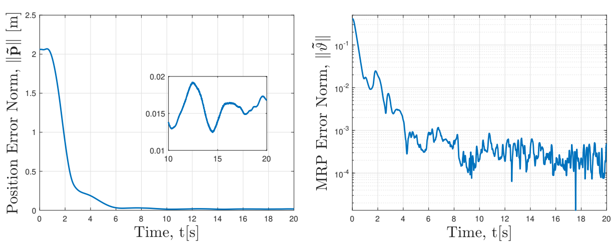

Fig. 2. Position and MRP error norm evolution during trajectory tracking in simulation. From left to right: (a) $\|\tilde{\mathbf{p}}\|$, (b) $\|\tilde{\boldsymbol{\vartheta}}\|$.

From Fig. 3, one can observe that the position control law saturation functions operated within the saturated region during the initial phase of the simulation. Nonetheless, the quadrotor smoothly converged to the desired trajectory.

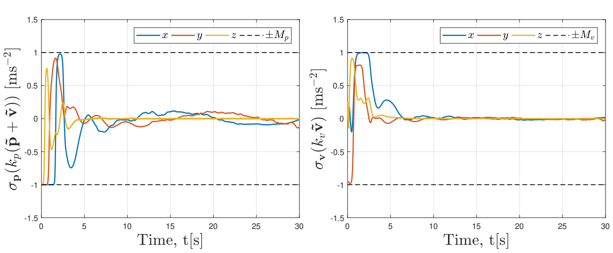

Fig. 3. Saturation terms of $\mathbf{u_p}$ during trajectory tracking in simulation. From left to right: (a) $\boldsymbol{\sigma_p}\left(k_p\left(\tilde{\mathbf{p}}+\tilde{\mathbf{v}}\right)\right)$, (b) $\boldsymbol{\sigma_v}\left(k_v\tilde{\mathbf{v}}\right)$.

VII. CONCLUSION

A novel backstepping controller was proposed to tackle the trajectory tracking problem for quadrotors. The strategy was designed based on the hybrid system theory, comprises a saturated position control law, and exploits the unique properties of the MRP representation. The resulting control structure is robust to small measurement noise and renders the full system error dynamics globally asymptotically stable. In this way, the proposed methodology is able to perform a position trajectory while minimizing the angular distance to the desired rotation matrix. The simulation results demonstrated this capacity, validating, thereby, the devised solution.

VIII. ACKNOWLEDGMENTS

This work was supported by FCT, through IDMEC, under LAETA, project UIDB/50022/2020. L. Martins holds a scholarship from the FCT project DECENTER [LISBOA-01-0145-FEDER-029605], funded by the Lisboa 2020 and PIDDAC programs.

REFERENCES

[1] C. G. Mayhew, R. G. Sanfelice, and A. R. Teel, "Quaternion-based hybrid control for robust global attitude tracking," *IEEE Transactions on Automatic control*, vol. 56, no. 11, pp. 2555–2566, 2011.

[2] T. Lee, "Global exponential attitude tracking controls on so(3)," *IEEE Transactions on Automatic Control*, vol. 60, no. 10, pp. 2837–2842, 2015.

[3] J. L. Junkins and H. Schaub, *Analytical Mechanics of Space Systems*. American Institute of Aeronautics and Astronautics, 2009.

[4] H. Gui and G. Vukovich, "Robust switching of modified rodrigues parameter sets for saturated global attitude control," *Journal of Guidance, Control, and Dynamics*, vol. 40, no. 6, pp. 1529–1542, 2017.

[5] E. Frazzoli, M. A. Dahleh, and E. Feron, "Trajectory tracking control design for autonomous helicopters using a backstepping algorithm," in *Proceedings of the 2000 American Control Conference. ACC (IEEE Cat. No. 00CH36334)*, vol. 6. IEEE, 2000, pp. 4102–4107.

[6] E. Lefeber, S. van den Eijnden, and H. Nijmeijer, "Almost global tracking control of a quadrotor uav on se(3)," in *2017 IEEE 56th Annual Conference on Decision and Control (CDC)*, 2017, pp. 1175–1180.

[7] W. Lei, C. Li, and M. Z. Q. Chen, "Robust adaptive tracking control for quadrotors by combining pi and self-tuning regulator," *IEEE Transactions on Control Systems Technology*, vol. 27, no. 6, pp. 2663–2671, 2019.

[8] S. Bhat and D. Bernstein, "A topological obstruction to continuous global stabilization of rotational motion and the unwinding phenomenon," *Systems & Control Letters*, vol. 39, no. 1, pp. 63–70, 2000.

[9] P. Casau, R. G. Sanfelice, R. Cunha, D. Cabecinhas, and C. Silvestre, "Robust global trajectory tracking for a class of underactuated vehicles," *Automatica*, vol. 58, pp. 90–98, 2015.

[10] C. G. Mayhew, R. G. Sanfelice, and A. R. Teel, "On path-lifting mechanisms and unwinding in quaternion-based attitude control," *IEEE Transactions on Automatic Control*, vol. 58, no. 5, pp. 1179–1191, May 2013.

[11] R. Naldi, M. Furci, R. G. Sanfelice, and L. Marconi, "Robust global trajectory tracking for underactuated vtol aerial vehicles using inner-outer loop control paradigms," *IEEE Transactions on Automatic Control*, vol. 62, no. 1, pp. 97–112, 2017.

[12] R. Goebel, R. G. Sanfelice, and A. R. Teel, "Hybrid dynamical systems," *IEEE control systems magazine*, vol. 29, no. 2, pp. 28–93, 2009.

[13] R. Goebel, R. G. Sanfelice, and A. Teel, *Hybrid dynamical systems: modeling, stability, and robustness*. Princeton University Press, 2012.

[14] R. Mahony, V. Kumar, and P. Corke, "Multirotor aerial vehicles: Modeling, estimation, and control of quadrotor," *IEEE Robotics Automation Magazine*, vol. 19, no. 3, pp. 20–32, 2012.

[15] A. R. Teel, "Global stabilization and restricted tracking for multiple integrators with bounded controls," *Systems & control letters*, vol. 18, no. 3, pp. 165–171, 1992.

[16] S. Gayaka, L. Lu, and B. Yao, "Global stabilization of a chain of integrators with input saturation and disturbances: A new approach," *Automatica*, vol. 48, no. 7, pp. 1389–1396, 2012.

[17] H. K. Khalil and J. W. Grizzle, *Nonlinear systems*. Prentice hall Upper Saddle River, NJ, 2002, vol. 3.

[18] L. Martins, C. Cardeira, and P. Oliveira, "Feedback linearization with zero dynamics stabilization for quadrotor control," *Journal of Intelligent & Robotic Systems*, vol. 101, no. 1, pp. 1–17, 2021.